

Morphology of step structures on CeO₂(111)

Stefan Torbrügge, Marion Cranney, and Michael Reichling^{a)}

Fachbereich Physik, Universität Osnabrück, Barbarasträße 7, 49076 Osnabrück, Germany

(Received 28 May 2008; accepted 22 July 2008; published online 22 August 2008)

The morphology of step structures on the CeO₂(111) surface is studied by dynamic scanning force microscopy (SFM) operated in the noncontact mode. The surface exhibits hexagonal islands and pits of O–Ce–O triple layer height with steps mostly enclosing an angle of 120°. Atomically resolved images reveal that the (111) surface almost exclusively exhibits alternating steps having (110) and (001) facets. Kink sites and missing oxygen atoms at step edges are identified to be the dominating defective sites at step edges. It is demonstrated that low coordinated oxygen atoms at step edges can be removed by the scanning SFM tip. © 2008 American Institute of Physics.

[DOI: 10.1063/1.2969790]

Oxide surfaces and metals dispersed on oxide supports are widely used in catalytic applications.¹ The catalytic reactivity is strongly related to surface defects, where oxygen vacancies and step edges play a most important role, specifically for nanoparticles used in catalysis. While many experimental and theoretical studies conducted on metal oxide surfaces have been focused on the structure and reactivity of surface oxygen vacancies, much less studies have been reported on the characterization of step edges,^{2,3} mainly due to difficulties in investigating step edges with atomic resolution.

Ceria (CeO₂) holds substantial promise for solid-fuel cell technology and other catalytic applications, mainly for the production of hydrogen and oxidation of carbon monoxide.⁴ Understanding of both oxygen vacancies and step structures is most relevant for optimizing the activity of CeO₂ catalysts. Oxygen vacancy defects on the CeO₂(111) surface have been studied in detail by means of scanning tunneling microscopy⁵ (STM) and dynamic scanning force microscopy (SFM) operated in the noncontact mode.⁶ However, little is known about step edges on the CeO₂(111) surface, even though STM studies on thin CeO₂ films show that step edges are the dominating nucleation sites for gold clusters deposited at submonolayer coverage,⁷ underlining the importance of step edges for noble metal dispersion.

In this letter, we elucidate the structure of step edges on the CeO₂(111) surface using SFM. Atomically resolved images of step structures reveal that the (111) surface almost exclusively exhibits steps with (001) and (110) nanofacets. Additionally, kink sites and missing oxygen atoms at step edges are identified to be the dominating defective sites at step edges. We also find that low coordinated oxygen atoms can be manipulated by the SFM tip during scanning. Our results confirm the general notion that the step formation energy on metal oxides scales with the surface energy of the extended facet.^{2,3}

Experiments were carried out with a modified commercial ultrahigh vacuum SFM (Ref. 8) operated at room temperature with the frequency modulation detection method,⁹ keeping the cantilever oscillation amplitude constant and the tip-surface electrostatic interaction minimized.¹⁰ We studied the surface morphology of CeO₂ single crystals (Commercial

Crystal Laboratories), where the CeO₂(111) surface was prepared *in situ* by repeating cycles of Ar⁺ ion sputtering (1.5 kV, 4 × 10⁻⁵ mbar, 3 min) at room temperature with subsequent annealing of the sample for 2 min at 1225 K. Afterwards the sample was postannealed for an additional 60 min at 600 K, resulting in the formation of large terraces and smooth step edges. Tip preparation is described elsewhere.⁸

A large scale topographic SFM image of the CeO₂(111) surface is shown in Fig. 1(a). Large atomically flat terraces are separated by steps with a height of 0.31 nm corresponding to the height of a O–Ce–O triple layer [Fig. 1(b)]. The atomic resolution image from Fig. 1(c) shows the (1 × 1) termination of the surface as highlighted by the model in Fig. 1(d). In previous work, we demonstrated that in SFM studies on CeO₂(111) most likely the topmost layer of the oxygen terminated surface is imaged.⁶ Edges of regular step structures in Fig. 1(a) enclose an angle of 120°, resulting in the formation of the characteristic surface morphology exhibiting hexagonally shaped pits [Figs. 1(a)i and 1(a)ii] and is-

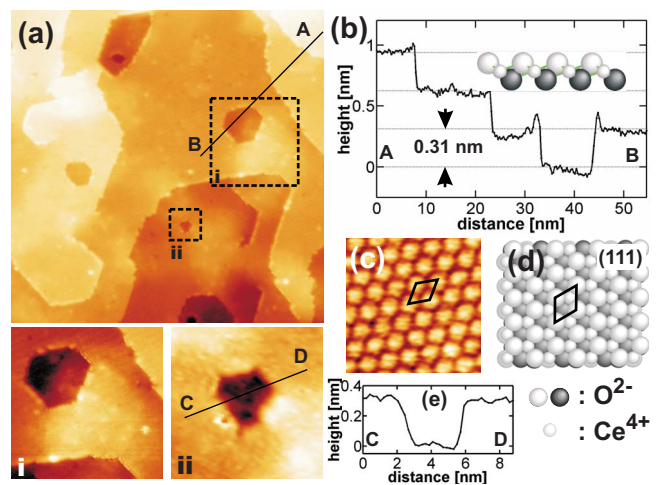


FIG. 1. (Color online) (a) Topographic SFM images of the CeO₂(111) surface morphology observed directly after preparation. (b) Height profile taken along the straight line in (a) revealing steps of triple-layer height. (c) Atomically resolved image together with a schematic model (d) of the stoichiometric oxygen terminated (111) surface. (e) Height profile as indicated in (a)ii. Imaging parameters: $f_0=296698$ Hz, $k=42$ N/m, $A=42.8$ nm, (a) image size (100 × 100) nm², $\Delta f=-1$ Hz. (c) image size (2.3 × 2.3) nm², $\Delta f=-5$ Hz.

^{a)}Electronic mail: reichling@uos.de.

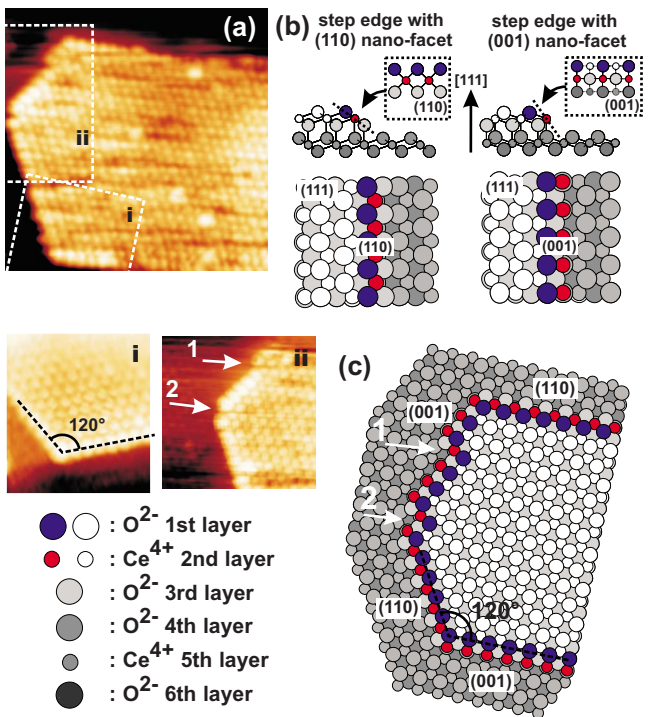


FIG. 2. (Color online) (a) Topographic SFM image of a hexagonal island structure. (a)i highlights the characteristic step angle of 120° . (a)ii shows frequently observed defects at step edges. (b) Top and profile view of schematic models of step edges on the $\text{CeO}_2(111)$ surface exhibiting (110) and (001) nanofacets. Insets give views onto the facets of the step edges as indicated by dashed lines in the profile view. (c) Model of the hexagonal island structure constructed from step edges in (b) explaining the surface morphology and frequently observed defects at step edges such as kink sites (1) and missing oxygen atoms (2). Imaging parameters: $f_0=79988$ Hz, $k=2.8$ N/m. (a) image size 10×10 nm², $\Delta f=-21.2$ Hz. (a)i image size (4×4) nm², (a)ii (6×6) nm², $\Delta f=-22.3$ Hz.

lands, whereas hexagonal pits again exhibit a depth corresponding to a triple layer [Fig. 1(e)]. This is in accordance with previously reported SFM studies on bulk crystals^{11,12} and STM studies on thin CeO_2 films^{13,14} underlining the generality of this morphology for (111) orientated CeO_2 surfaces prepared under conditions of thermal equilibrium. In the following, we elucidate the origin for this characteristic surface morphology.

An atomic resolution image of a hexagonal island is shown in Fig. 2(a). A detailed view on two inclining step edges shown in Fig. 2(a)i reveals that step edges are running along the close packed oxygen rows in $\langle 110 \rangle$ directions defining the characteristic angle of 120° . In Figs. 2(b) and 2(c), we assemble models of step edges running along the close packed oxygen rows. These models are constructed following a concept assuming structures with more highly coordinated atoms to be energetically more stable than those with less coordinated atoms.^{2,3} For the (111) surface, O atoms in the terminating layer are threefold coordinated. Thus we expect step structures exhibiting threefold coordinated oxygen atoms at step edges to be more stable than structures having lower coordinated oxygens. Due to the threefold surface symmetry of the (111) surface, only two distinct step edges can be constructed which are terminated by threefold coordinated oxygen atoms at the step. The two constructed step edges exhibit nanofacets of (001) and (110) surface terminations, as shown in Fig. 2(b) in top and profile view. First-principles calculations have shown that the order of stability

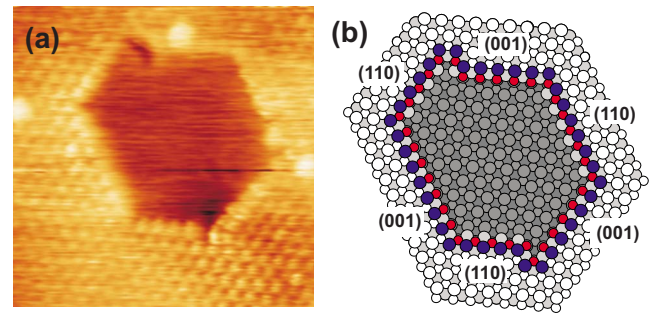


FIG. 3. (Color online) (a) Atomically resolved topographic SFM images of a hexagonal pit with (b) corresponding model. The notation is the same as in Fig. 2. Imaging parameters: $f_0=74590$ Hz, $k=2.8$ N/m, $A=39.3$ nm, image size (7×7) nm², $\Delta f=-7.3$ Hz.

of the low index CeO_2 surfaces is $E_{(111)} < E_{(110)} < E_{(001)}$.¹⁵ Thus the constructed models agree well with the concept that the step formation energy on metal oxides scales with the surface energy of the extended facet. This concept has already been applied to explain the surface morphologies of anatase $\text{TiO}_2(101)$ ³ and Zn-terminated $\text{ZnO}(0001)$.¹⁶

When constructed by this rule, steps of different types hit each other with an angle of 120° in agreement with the experimental observation. This is demonstrated in Fig. 2(c) where the model resembles the atomic arrangement of the hexagonal island shown in Fig. 2(a). Within the derived model it is also straightforward to explain the structure of kink sites as the one indicated by arrow (1) in Fig. 2(a)ii and the missing terminating oxygen atom at one vertex of the hexagonal island indicated by arrow (2).

Following the building rule further it is straightforward to describe the structure of frequently observed hexagonal pits. In Fig. 3(a) we show atomic details of such a hexagonal pit together with the corresponding structural model in Fig. 3(b). Again it is evident that the hexagonal surface structure of the $\text{CeO}_2(111)$ surface originates from alternating step edges exposing (001) and (110) nanofacets.

Our findings indicate that the hexagonal surface structure formation originates from thermodynamic equilibrium favoring energetically stable step edges having (001) and (110) facets. The observation of large terraces showing compact hexagonal islands and pits is attributed to an approach toward the equilibrium stage of the surface upon annealing, which is characterized by a decrease of total step length, since the (111) surface termination is the energetically most stable.¹⁵ However under conditions of thermal equilibrium one would expect the formation of triangular surface structures, in the case that one type of step edge is thermodynamically more stable than the other. The morphology of step structures on the $\text{CaF}_2(111)$ surface—having the same crystallographic geometry as $\text{CeO}_2(111)$ —has been studied with different thermal treatments.¹⁷ After cleavage at room temperature lightning-shaped arrangements having inclination angles of steps of 45° are observed and explained by local energy minimization upon cleavage. Upon thermal annealing, the cleavage topography was found to transform into a topography with trigonal and hexagonal islands due to preferential formation of two step types of $\langle 110 \rangle$ orientation and finally into a surface structure consisting of trigonal islands and pits. The formation of only one step type has been attributed to further minimization of the surface energy.^{17,18} On the $\text{CeO}_2(111)$ surface, however, trigonal islands and pits are

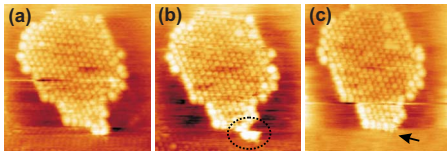


FIG. 4. (Color online) Sequence of topographic SFM images [(a)–(c)] showing the manipulation of low coordinated oxygen atoms at kink sites. The arrow in (c) indicates the removal of two atoms encircled in (b) at a kink on the lower step. Imaging parameters: $f_0=74740$ Hz, $k=2.8$ N/m, $A=37.6$ nm; [(a)–(c)] image size (9×9) nm², $\Delta f=-11.2$ Hz.

not found indicating that for the surface upon annealing in chemical equilibrium both step types presented in Fig. 2(b) coexist. We suggest two different explanations for this observation. First, the interaction between closely neighboring steps of different terminations may act as a kinetic hindrance for a transformation into triangular equilibrium shape¹⁷ at annealing temperatures applied in our experiments. Second, the step formation energies may in fact be very close together. This is supported by a statistical analysis¹⁹ of the length ratio of (110) and (001) faceted step edges measured for hexagonal islands and pits, as shown in Figs. 1(a)i, 1(a)ii, and 3 yielding a value of (1.09 ± 0.14) . Within the measurement accuracy this value suggests an almost equal step formation energy for both step terminations. To elucidate the two scenarios further, theoretical modeling of step structures on CeO₂(111) is required.

Besides almost defect free step edges, as shown in Fig. 2, more defective step structures exposing a considerable amount of low coordinated atoms at kink sites are frequently observed. Figure 4(a)–4(c) display a series of three consecutively recorded images of a hexagonal island structure with a high density of kink sites and missing oxygens at steps. Within the series of images it is found that step edge atoms are manipulated by the tip. The arrow in (c) indicates the removal of two atoms encircled in (b) at a kink on the lower step.

In summary, our results confirm the notion that step formation energy on metal oxides scales with the surface energy of the extended facet,³ and that this general concept can be extended to rare-earth oxides such as CeO₂. Our finding that step edges exposing (001) and (110) nanofacets are predominantly formed on the (111) surface has important implications for the understanding of the structure and reactivity of CeO₂ nanoparticles possessing mainly {111} surfaces.²⁰ For example in first-principles calculations, the adsorption of CO on the low index CeO₂ surfaces has been found to strongly depend on the surface termination resulting in a strong chemisorption on the (110) and weak physisorption on the

(111) surface.²¹ Thus it is suggested that the oxidation of CO via the creation of an oxygen vacancy ($\text{CO} + \text{O}_{\text{lat}} \rightarrow \text{CO}_2 + \text{O}_{\text{vac}}$) on the (111) terminated surface is predominantly taking place at step edges exposing (110) nanofacets. Furthermore, we find that low coordinated oxygen atoms at kink sites can be manipulated by the SFM tip during scanning, indicating that these atoms are more weakly bound. Upon annealing, oxygen release may preferably take place at these sites. We hope that our studies will stimulate further theoretical work of the interaction of noble metals and adsorbates with step edges on CeO₂ surfaces.

Financial support by the Deutsche Forschungsgemeinschaft is gratefully acknowledged.

¹V. E. Henrich and P. A. Cox, *The Surface Science of Metal Oxides* (Cambridge University Press, Cambridge, 1996).

²V. E. Henrich and S. K. Shaikhutdinov, *Surf. Sci.* **574**, 306 (2005).

³X. G. Gong, A. Selloni, M. Batzill, and U. Diebold, *Nat. Mater.* **5**, 665 (2006).

⁴A. Trovarelli, *Catal. Rev. - Sci. Eng.* **38**, 439 (1996).

⁵F. Esch, S. Fabris, L. Zhou, T. Montini, C. Africh, P. Fornasiero, G. Comelli, and R. Rosei, *Science* **309**, 752 (2005).

⁶S. Torbrügge, M. Reichling, A. Ishiyama, S. Morita, and O. Custance, *Phys. Rev. Lett.* **99**, 056101 (2007).

⁷J. L. Lu, H. J. Gao, S. Shaikhutdinov, and H. J. Freund, *Catal. Lett.* **114**, 8 (2007).

⁸S. Torbrügge, J. Lübke, L. Tröger, M. Cranney, T. Eguchi, Y. Hasagawa, and M. Reichling, *Rev. Sci. Instrum.* **79**, 083701 (2008).

⁹T. R. Albrecht, P. Grütter, D. Horne, and D. Rugar, *J. Appl. Phys.* **69**, 668 (1991).

¹⁰S. Gritschneider and M. Reichling, *Nanotechnology* **18**, 044024 (2007).

¹¹K. Fukui, Y. Namai, and Y. Iwasawa, *Appl. Surf. Sci.* **188**, 252 (2002).

¹²S. Gritschneider, Y. Namai, Y. Iwasawa, and M. Reichling, *Nanotechnology* **16**, S41 (2005).

¹³S. Eck, C. Castellarin-Cudia, S. Surnev, M. G. Ramsey, and F. P. Netzer, *Surf. Sci.* **520**, 173 (2002).

¹⁴J. L. Lu, H. J. Gao, S. Shaikhutdinov, and H. J. Freund, *Surf. Sci.* **600**, 5004 (2006).

¹⁵M. Nolan, S. Grigoleit, D. C. Sayle, S. C. Parker, and G. W. Watson, *Surf. Sci.* **576**, 217 (2005).

¹⁶F. Ostendorf, S. Torbrügge, and M. Reichling, *Phys. Rev. B* **77**, 041405(R) (2008).

¹⁷J. B. Engelhardt, H. Dabringhaus, and K. Wandelt, *Surf. Sci.* **448**, 187 (2000).

¹⁸V. E. Puchin, A. V. Puchina, M. Huisinga, and M. Reichling, *J. Phys.: Condens. Matter* **13**, 2081 (2001).

¹⁹Each hexagonal island or pit consists of six alternating steps having (110) and (001) facets [see Fig. 3]. We sum the measured length of the three steps having the same facet and calculate the total length ratio for each hexagonal structure. In total 52 hexagonal islands and pits are considered and the mean value and standard deviation of the whole data set are computed.

²⁰F. Zhang, Q. Jin, and S. W. Chan, *J. Appl. Phys.* **95**, 4319 (2004).

²¹Z. X. Yang, T. K. Woo, and K. Hermansson, *Chem. Phys. Lett.* **396**, 384 (2004).